JCTC Journal of Chemical Theory and Computation

Article

pubs.acs.org/JCTC

An Improved Isotropic Periodic Sum Method That Uses Linear Combinations of Basis Potentials

Kazuaki Z. Takahashi,*[,†] Tetsu Narumi,[‡] Donguk Suh,[†] and Kenji Yasuoka*[,†]

[†]Department of Mechanical Engineering, Keio University, Yokohama 223-8522, Japan

[‡]Department of Computer Science, University of Electro-Communications, Tokyo 182-8585, Japan

Supporting Information

ABSTRACT: Isotropic periodic sum (IPS) is a technique that calculates long-range interactions differently than conventional lattice sum methods. The difference between IPS and lattice sum methods lies in the shape and distribution of remote images for long-range interaction calculations. The images used in lattice sum calculations are identical to those generated from periodic boundary conditions and are discretely positioned at lattice points in space. The images for IPS calculations are "imaginary", which means they do not explicitly exist in a simulation system and are distributed isotropically and periodically around each particle. Two different versions of the original IPS method exist. The IPSn method is applied to calculations for point charges, whereas the IPSp method calculates polar molecules. However, both IPSn and IPSp have their advantages and disadvantages in simulating bulk water or water−vapor interfacial systems. In bulk water systems, the cutoff radius effect of IPSn strongly affects the configuration, whereas IPSp does not provide adequate estimations of water−vapor interfacial systems unless very long cutoff radii are used. To extend the applicability of the IPS technique, an improved IPS method, which has better accuracy in both homogeneous and heterogeneous systems has been developed and named the linear-combination-based isotropic periodic sum (LIPS) method. This improved IPS method uses linear combinations of basis potentials. We performed molecular dynamics (MD) simulations of bulk water and water−vapor interfacial systems to evaluate the accuracy of the LIPS method. For bulk water systems, the LIPS method has better accuracy than IPSn in estimating thermodynamic and configurational properties without the countercharge assumption, which is used for IPSp. For water−vapor interfacial systems, LIPS has better accuracy than IPSp and properly estimates thermodynamic and configurational properties. In conclusion, the LIPS method can successfully estimate homogeneous and heterogeneous systems of polar molecular systems with good accuracy.

1. INTRODUCTION

Recent computational advancements make it possible to carry out large-scale molecular dynamics (MD) simulations such as biological and polymer systems that need more than 10^5−10^9 molecules. However, 10^5−10^9 molecules are insufficient to express actual phenomena because nature typically contains on the order of 10^{23} molecules. The effect of long-range interactions, which do not converge within finite distances, is also important to estimate thermodynamic, structural, and dynamical properties. Interaction calculations for all molecular pairs in systems that contain 10^{23} molecules are prohibitive. To avoid this difficulty, periodic boundary conditions (PBCs) are used to model the effect of an infinitely large domain. There are approximation methods, such as cutoff-like methods and lattice sum methods, for systems with PBCs that estimate long-range interactions.

Cutoff-like methods are often used to reduce the cost of long-range interaction calculations. The interactions between molecular pairs only with a distance shorter than a given cutoff length are considered, and effects from more distant pairs are considered by a bulk structure or are simply neglected. The cutoff with or without the switch function (SF) and the reaction field (RF) method are some examples of typical cutoff-like methods for Coulombic systems. Simulations can be accelerated by using cutoff-like methods, but truncation or continuum approximation of long-range interactions have serious defects for various systems. In Lennard-Jones fluid systems, long-range interactions do not have a prominent effect on transport properties,[1,2] but phase equilibria and interfacial properties change drastically.[3−5] In water systems, electrostatic interactions dominate the physical properties, and truncation or continuum approximation may lead to unphysical results. The plain cutoff, SF, and RF methods using dipolar approximation offer insufficient accuracy,[6−16] and all of the results are highly sensitive to the cutoff distance. The RF method with a higher-order Kirkwood expansion can diminish this cutoff radius effect, with a relatively large cutoff radius.[17−19] Cutoff-like methods are also applied to macromolecular systems,[20−32] and many results indicate the aforementioned approximations have difficulties when estimating these systems.

The Ewald sum[33] is one of the most accurate and standard lattice sum methods for calculating long-range interactions. It incorporates PBCs by use of discrete Fourier transform, but the reciprocal term is computationally expensive, for it has a $O(N^{3/2})$ computational cost. Particle mesh Ewald (PME)[34] and smooth particle mesh Ewald (SPME)[35] are particle−particle/particle−mesh (PPPM) approaches that use the fast Fourier transform (FFT) for the Ewald sum. PPPM has $O(N \log N)$ computational cost and performs well on intermediate systems[36] ($N \sim 10^3$−10^5). However, PME is difficult to use for large systems ($N \geq 10^6$), which require the computational

Received: May 14, 2012
Published: September 6, 2012

power of massively parallel heterogeneous computers. On parallel computers, the inherent parallelism of the underlying algorithm becomes important. FFT has problems achieving strong scaling on massively parallel machines.[37−39] Since PME relies on FFT, similar results are expected. The tree-based method[40,41] can achieve higher parallelism than FFT due to omission of the reciprocal space calculations. This method was first developed by Barnes and Hut[40] (BH tree-code), and it has $O(N \log N)$ computational cost. The fast multipole method (FMM)[41] is an advanced BH tree-code for faster calculations of long-range interactions. The calculation cost of FMM is $O(N)$, so applications of very large scales will benefit the most. The tree-based method has already been applied to the field of molecular simulations[17−19,37,42−49] as one of the representative methods to calculate long-range interactions. The biggest advantage of tree-based methods is that a higher parallelism can be achieved in comparison with FFT. Even with highly parallel computers, most of the communication of the tree-based method is between the nearest-neighbor nodes, and the amount of communication between remote nodes becomes smaller as the distance between nodes becomes larger. The parallel execution of FFT requires all-to-all communication between nodes, which greatly reduces the parallel efficiency because the communication performance between distant nodes are much slower than that of closer nodes in current massively parallel computers. Yokota et al.[38] carried out petascale turbulence simulations using 2048 graphic processing units (GPUs) for 2048^3 particles to compare the parallel efficiency of FMM and FFT, and the results clearly show the superiority of FMM. On the other hand, the disadvantage of the tree-based method in comparison with Ewald sum is that it does not consider infinite periodic systems. Since contributions from only a finite number of periodic cells are calculated, it can be interpreted as having a very large cutoff volume or radius. Therefore, the tree-based method can be regarded as an extreme case of a cutoff-like method, while it is originally a lattice sum method. In spite of the large cutoff radius of the tree-based method, the effect of the cutoff should be treated carefully.

The isotropic periodic sum (IPS) method was first developed by Wu and Brooks.[50−52] In the IPS method, the approximated long-range effect from interactions is included in the potential function, so the algorithm of the interaction calculation is similar to that of the cutoff-like method. The difference between the IPS method and lattice sum method lies in the shape and distribution of remote images for long-range interaction calculations. The images used in lattice sum calculations are identical to those generated from periodic boundary conditions and are discretely positioned at lattice points in space. The images for IPS calculations are "imaginary", which means they do not explicitly exist in a simulation system and are distributed isotropically and periodically around each particle. Since the treatment of the effect from image cells between the IPS and lattice sum methods is basically different, the expressions for the long-range term of the potential function of these two methods are naturally different. Furthermore, the IPS method can avoid reciprocal space calculations, which arise from the long-range term of the Ewald sum and are expressed by a Fourier series. The algorithm for the interaction calculation of the IPS method is completely the same as that of the cutoff method, except that the isotropic periodic long-range effect is included in the pairwise potential. Therefore, the IPS method is a method that can calculate contributions from the infinite periodic structure without reciprocal space calculations. Two different versions of the original IPS method have been developed by Wu and Brooks.[50,52] The IPSn method is applied to calculations for point charges, whereas the IPSp method calculates polar molecules. Overall, the IPS method has been applied to Lennard-Jones fluids,[50,53] bulk water,[54,55] water−vapor interfaces,[56,57] and lipid[56,58] systems.

Previous studies for bulk water systems[52,54,55] indicate difficulties for the IPSn method in calculating polar molecular systems. In order to avoid this problem, Wu and Brooks[52] developed the IPSp method, which is a modified IPS method for polar molecular systems. The principal difference between IPSn and IPSp is the inclusion of a countercharge effect. In polar systems, a countercharge exists around a particle that has a charge. The pairwise potential of the IPSp method includes a screening effect from the countercharge. The IPSp potential for Coulombic interactions successfully avoids this problem when predicting the configuration of water and other polar molecules. Wu and Brooks[51,52] found that the results of both IPSn and IPSp methods are almost the same as that of the Ewald sum for estimating the electrostatic configuration of water−vapor interfacial systems at relatively large cutoff radii, which is equal to twice the length of the longest simulation box dimension, $2L_z$. In order to make suggestions for a minimum cutoff radius estimation of interfacial systems, we carried out MD simulations of water−vapor interfacial systems using IPSn and IPSp in our previous study.[57] The details of the cutoff radius effect at $L_z/6 \leq r_c \leq L_z/2$ were evaluated for the IPSn and IPSp methods, and we have found two problems in the conventional IPS techniques. One is the eccentric deviation of the surface tension when the IPSn method is used at a certain cutoff radius. This poor estimation of the surface tension can be a source of a fatal error for simulations of complex membrane systems. The other is the fact that the convergence of surface tension and electrostatic configuration for the IPSp method is considerably slower than that for the IPSn method. The cause of this poor estimation for the IPSp method is an unphysical behavior of the screening effect around molecules on the interfacial surface. The convergence of interfacial properties for the IPSn method is faster than that for IPSp, but an eccentric deviation of surface tension occurs. Therefore we had concluded that the IPSn method gives superior results for estimation of interfacial systems. In spite of the difference in convergence for the IPSn and IPSp methods, both versions of the IPS method require a long cutoff radius for simulations of interfacial systems. For long-cutoff calculations by the IPS method, the IPS/DFFT method has also been developed by Wu and Brooks.[51] The method is a combination of the IPS method and FFT, and it has $O(N \log N)$ computational cost. IPS/DFFT can reduce the calculation cost when one has to choose a long cutoff radius, because the method requires less wavenumber calculations than that of PME.[51] Therefore the method works quite well for intermediate systems. For large systems that require massively parallel computers, we developed the IPS/Tree method[59] in our previous work. The method is a combination of IPS and the tree-based method for long-cutoff calculations without FFT. IPS/Tree has superior efficiency for massively parallel computers compared to PME and IPS/DFFT while maintaining the infinite isotropic periodic structure that is not considered in conventional tree-based methods.

Long-cutoff calculation methods for the IPS technique have distinct advantages in comparison with conventional lattice sum

methods; however, the cutoff radius dependence of the IPS method still remains a problem. As stated earlier, in bulk water systems, the cutoff radius of IPSn strongly affects the configuration, whereas IPSp does not provide adequate estimations of water−vapor interfacial systems unless very long cutoff radii are used.

In this paper, we propose an improved IPS method using the linear combination of basis potentials (linear-combination-based isotropic periodic sum, LIPS) based on an extended isotropic periodic summation theory. The LIPS method successfully extends the range of application of the IPS technique; this method can accurately estimate both homogeneous and heterogeneous systems for nonpolar and polar molecules. The algorithm of the LIPS method for interaction calculations is the same as that of the conventional IPS method, regardless of the extension of the isotropic periodic summation theory. Therefore, IPS techniques with long cutoff radii, such as IPS/DFFT and IPS/Tree, can be easily assimilated with the LIPS method. Our LIPS method offers improvements in both accuracy and calculation speed. We performed MD simulations of bulk water and water−vapor interfacial systems to evaluate the accuracy of the LIPS method and compared them to those of the IPSn, IPSp, and Ewald sum methods. In bulk water systems, the potential energy, self-diffusion coefficient, radial distribution function, and distance dependence of the Kirkwood factor were mainly calculated. In water−vapor interfacial systems, the potential energy, surface tension, electric potential profile, and dipole orientational function were calculated. To carefully evaluate the cutoff radius effect of the LIPS method, all physical properties above were calculated for many different cutoff radii.

2. THEORIES AND METHODS

2.1. Extended IPS Theory for LIPS Method Development. The fundamental concept for all IPS techniques—IPSn, IPSp, and LIPS—starts from dividing the total potential energy U_i of a nonbonded interaction for particle i into two parts: local region interactions within Ω_i and long-range interactions outside Ω_i. The effect of long-range interactions outside Ω_i becomes a function of the configuration of Ω_i, $\phi(r_{ij},\Omega_i)$:

$$U_i = \frac{1}{2}\sum_{r_j\in\Omega_i}[u(r_{ij}) + \phi(r_{ij}, \Omega_i)] \quad (1)$$

where r_j is the position of particle j, r_{ij} is the vector from particle i to particle j, and $u(r_{ij})$ is the potential energy for r_{ij}. For typical cutoff methods, $\phi(r_{ij},\Omega_i)$ is simply ignored or is applied to the long-range correction term based on continuum approximations. On the other hand, for IPS techniques, $\phi(r_{ij},\Omega_i)$ is represented by r_c along with other parameters that depend on the formulation of interactions with IPS techniques. It is clear that the treatment of constraint conditions for the IPS technique greatly affects estimation of homogeneous and heterogeneous systems.[54,55,57] In the IPSn method, the distribution of isotropic periodic images assume three effective interaction potentials: a contribution from the axial images, random images, and the original pairwise potential. The pairwise potential of the IPS method is derived from these three effective interactions and only one cutoff boundary condition (see section 1 of Supporting Information). IPSp has one additional effective potential, which expresses the counter-charge effect, and has two additional cutoff boundary conditions for dipoles. In the improved method, instead of one axial image, the extended IPS theory models numerous directional images along with the axial images. If the number of directional images is l, $l + 2$ effective interaction potentials of the extended IPS theory exist, where potential energies from l directional images are the basis potentials, plus one random image and one original pairwise potential. The potential energy of LIPS is determined by these $l + 2$ effective potentials and $l + 1$ constraint conditions. These constraint conditions include cutoff boundary conditions for higher-order multipoles. The contributions from directional images are represented by the linear combination of basis potentials. Linear combination coefficients of the basis potentials are determined by solving equations that are given by constraint conditions. This clearly means that a new potential function of LIPS satisfies the constraint conditions, which include boundary conditions for higher-order multipoles.

Figure 1 shows the charge distribution from the extended IPS theory when focusing on interactions between particle i (charge q) and particle j (charge Q). As shown in Figure 1, a charge q has a local region around it. This local region has a spherical configuration with a radius r_c centered on the charge. The spherical shells centered at the charge are called isotropic periodic images. There are an infinite number of such shells around the charge that fill the space. The shells are labeled 1, 2, 3, ..., m, ... starting from the inside. The mth shell has a radius of $2mr_c$. Any charge Q in the local region interacts with particle i and all isotropic periodic images. In the extended IPS theory, the isotropic periodic images consist of l directional images (k = 1, 2, 3, ..., l) and one random image (shaded area in Figure 1). Each directional image provides a potential energy, $u_k(r_{ij},r_c,\theta_k)$, which is expressed by

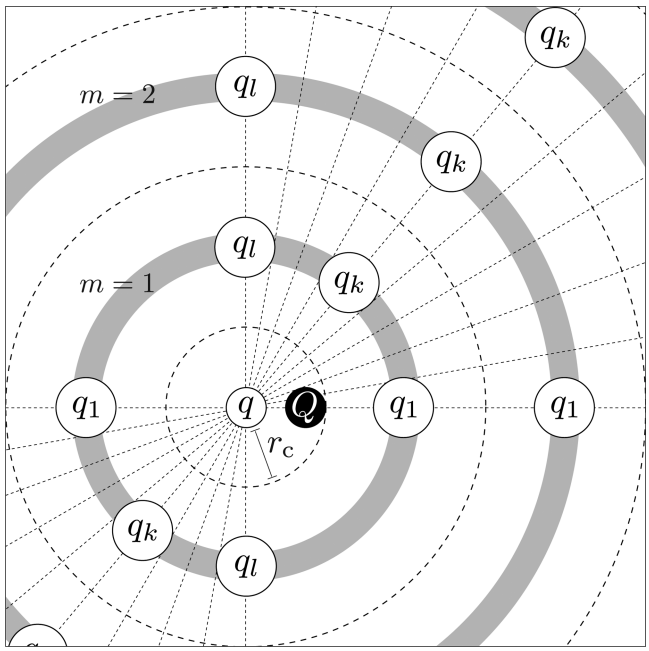

Figure 1. Distribution of isotropic periodic images for particle i in the extended IPS theory. Instead of axial images, directional images were assumed. Equation 2 requires the number of particles of each directional image within the mth shell to be 2, so each directional image within the mth shell has $2q_k$ charge, while shell images have $\{24m^2 + 2 - 2\sum_{k=1}^{l}(q_k/q)\}q$ charges. The mth shell contains in total $(24m^2 + 2)q$ charges.

dx.doi.org/10.1021/ct3003805 | J. Chem. Theory Comput. 2012, 8, 4503−4516

$$u_k(r, r_c, \theta_k) = \frac{Qq}{4\pi\varepsilon_0}\frac{q_k}{q} \sum_{m=1}^{\infty} \{(r^2 + 4m^2 r_c^2 - 4mr_c r \cos\theta_k)^{-1/2} + (r^2 + 4m^2 r_c^2 + 4mr_c r \cos\theta_k)^{-1/2}\} \equiv \frac{q_k}{q}\phi_k(r, r_c, \theta_k) \quad (2)$$

where q_k is the charge of the kth directional image, θ_k ($0 \le \theta_k \le \pi/2$) is the angle from the axial images ($\theta_k = 0$), and ε_0 is the permittivity of vacuum. Equation 2 requires the number of particles of each directional image within the mth shell to be 2, so each directional image within the mth shell has $2q_k$ charges, while shell images have $\{24m^2 + 2 - 2\sum_{k=1}^{l}(q_k/q)\}q$ charges. The mth shell contains in total $(24m^2 + 2)q$ charges. It should be noted that the distribution of whole charges on directional images does not need to satisfy the axial symmetry at a certain axis. As we will discuss in more detail in the next section (eqs 13−19), contributions from all effective potentials will finally provide an isotropic periodic surrounding environment, whereas the distribution of whole particles on directional images are generally anisotropic.

The potential energy from the random images, $u_{random}(r_{ij},r_c)$, is given by

$$u_{random}(r, r_c) = \frac{Qq}{4\pi\varepsilon_0} \sum_{m=1}^{\infty} \left[\{24m^2 + 2 - 2\sum_{k=1}^{l}(q_k/q)\}\frac{1}{2} \int_0^{\pi} (r^2 + 4m^2 r_c^2 - 4mr_c r \cos\theta)^{-1/2} \sin\theta \, d\theta \right] \equiv \phi_{random}(r, r_c) \quad (3)$$

If the number of directional images is l, then $l + 2$ effective interaction potentials—$u_k(r,r_c,\theta_k)$ ($k = 1, 2, 3, ..., l$), $u_{random}(r,r_c)$, and $u(r) = Qq/4\pi\varepsilon_0 r$—can be created for the extended IPS theory.

Equations similar to eqs 2 and 3 can be developed for any other type of potential, $u(r)$, that depends only on the distance r. These equations can be rewritten for $u(r)$:

$$u_k(r, r_c, \theta_k) = c_k \sum_{m=1}^{\infty} [u\{(r^2 + 4m^2 r_c^2 - 4mr_c r \cos\theta_k)^{1/2}\} + u\{(r^2 + 4m^2 r_c^2 + 4mr_c r \cos\theta_k)^{1/2}\}] \equiv c_k\phi_k(r, r_c, \theta_k) \quad (4)$$

$$u_{random}(r, r_c) = \sum_{m=1}^{\infty} \left[(24m^2 + 2 - 2\sum_{k=1}^{l} c_k)\frac{1}{2} \int_0^{\pi} u\{(r^2 + 4m^2 r_c^2 - 4mr_c r \cos\theta)^{1/2}\} \sin\theta \, d\theta \right] \equiv \phi_{random}(r, r_c) \quad (5)$$

where c_k is the linear combination coefficient of basis potentials. Therefore, the LIPS potential, $u_{LIPS}(r,r_c)$, can be expressed by

$$u_{LIPS}(r, r_c) = u(r) + \sum_{k=1}^{l} u_k(r, r_c, \theta_k) + u_{random}(r, r_c) = u(r) + \sum_{k=1}^{l} c_k\phi_k(r, r_c, \theta_k) + \phi_{random}(r, r_c) \equiv u(r) + \phi_{LIPS}(r, r_c) \quad (6)$$

We call the set of $\phi_k(r,r_c,\theta_k)$ basis potentials. The potential energy of LIPS is expressed by $u(r)$, $\phi_{random}(r,r_c)$, and the linear combination of basis potentials. One should note that $u_{LIPS}(r,r_c)$ is the pseudo pairwise potential that plays the same role as the IPS method. The LIPS pairwise potential already contains contributions from the surrounding environment. This is the basic concept of the IPS and LIPS method described in eq 1.

It should be noted that the summations in eqs 4 and 5 do not converge, so the configuration with $r = 0$ is used for the reference state, and LIPS potentials are calculated on the basis of the reference states:

$$\phi_{LIPS}(r, r_c) = \sum_{k=1}^{l} c_k\{\phi_k(r, r_c, \theta_k) - \phi_k(0, r_c, \theta_k)\} + \{\phi_{random}(r, r_c) - \phi_{random}(0, r_c)\} \quad (7)$$

This is the equivalent to the original IPS method (see section 1 of Supporting Information). Using a reference state will not change the force, and for neutral systems, it will not change the total electrostatic energy because the total sum of electrostatic energy at the reference state is zero.

In this work, we configure the cutoff boundary conditions and other matching conditions to determine c_k. The cutoff boundary conditions are given by

$$\frac{d^{k_b}}{dr^{k_b}}\{u(r) + \phi_{LIPS}(r, r_c)\}|_{r=r_c} = 0 \quad (k_b = 1, 2, 3, ..., n_b) \quad (8)$$

where n_b is the number of cutoff boundary conditions. These equations smooth the LIPS potentials, so the higher-order derivatives are zero on the cutoff boundary. The rationale of the zero value in the higher-order derivative at the cutoff boundary is to remove unphysical energy barriers and thus properly reproduce bulk systems. This is similar to the IPSp method.

The IPSp method prevents these energy barriers by including the countercharge effect. The countercharge effect of the IPSp is equal to boundary conditions to dipoles; that is, the second- and third-order differentials have zero value at the cutoff radius. However, as mentioned before, IPSp does not provide adequate estimations of water−vapor interfacial systems unless very long cutoff radii are used, because of the countercharge effect, whereas the IPSn method gives reasonable accuracy for estimation of water−vapor interfacial systems. Therefore, in order to extend the range of application of the IPS technique, from bulk systems to interfacial systems, it is desirable for the shape of LIPS potentials to be similar to the IPSn potential. Hence we set matching conditions for the shape of the LIPS potentials:

$$\frac{d^{k_m-1}}{dr^{k_m-1}}\phi_{LIPS}(r, r_c)|_{r=\alpha r_c} = \frac{d^{k_m-1}}{dr^{k_m-1}}\phi_{IPSn}(r, r_c)|_{r=\alpha r_c} \quad (k_m = 1, 2, 3, ..., n_m) \quad (9)$$

where $0 < \alpha < 1$, $\phi_{IPSn}(r,r_c)$ is the contribution from all isotropic periodic images for the IPSn method (see section 1 of Supporting Information), and n_m is the number of matching conditions for differentials. This equation requires $n_b \geq 2$ and $n_m \geq 1$. As stated earlier, higher order cutoff boundary conditions require a vastly different potential curve from that of IPSn, which is the as same as IPSp. To control this difference and obtain a similar curve as IPSn at $[0, \alpha r_c]$, we set n_m to be $n_b + 2$. This means that the smooth continuity of IPSn and the LIPS potential curve at $r = \alpha r_c$ is guaranteed for n_bth differential functions. When the number of equations is $n_b + n_m$, variables for LIPS are c_k ($k = 1, 2, 3, ..., l$) and α, so the following relationship is satisfied:

$$l + 1 = n_b + n_m \quad (n_b \geq 2, n_m \geq 1) \tag{10}$$

The LIPS potential is found when the simultaneous equations, which are established from eqs 6, 8, and 9, have a solution.

2.2. LIPS Coulombic Potential. For the Coulombic potential, $u(r) = Qq/4\pi\varepsilon_0 r$, $\phi_{LIPS}(r,r_c)$ in eq 6 can be expressed as

$$\phi_{LIPS}(r, r_c) = \frac{Qq}{4\pi\varepsilon_0}\left(-\frac{1}{2r_c}\right)\phi^*_{LIPS}(r/2r_c) = \frac{Qq}{4\pi\varepsilon_0} \frac{1}{2r_c}\left[\sum_{k=1}^{l} c_k\{\phi^*_k(r/2r_c, \theta_k) - \phi^*_k(0, \theta_k)\} + \{\phi^*_{random}(r/2r_c) - \phi^*_{random}(0)\}\right] \tag{11}$$

where $\phi^*_{LIPS}(r/2r_c)$ is reduced to $\phi_{LIPS}(r,r_c)$; $\phi^*_k(r/2r_c,\theta_k)$ is reduced to $\phi_k(r,r_c,\theta_k)$; and $\phi^*_{random}(r/2r_c)$ is reduced to $\phi_{random}(r,r_c)$.

Constraint conditions and basis potentials are decided by the principles stated in the previous section to determine the LIPS potentials. In this work, we set constraint conditions to eqs 8 and 9. The variable α, which is in eq 9, is useful to evaluate the shape of the LIPS potential. When α is determined, the shape of the LIPS potential, at least in the range $0 \leq r \leq \alpha r_c$, becomes the same as that of the IPSn potential. A larger α value means the LIPS potential becomes close to that of the IPSn potential, which implies that a larger α is the cause of poor estimation of bulk water systems. Therefore, we conducted a search on basis potentials that provide the smallest but most effective α. In this work, the basis potentials can be set by determining θ_k:

$$\theta_k = \theta_0 + \frac{k-1}{l-1}\theta_l \tag{12}$$

where $\theta_0 \geq 0$, $\theta_l > 0$, and $\theta_0 + \theta_l \leq \pi/2$. We particularly investigated the θ_k dependence of α at $\theta_0 = 0$, since basis potentials give relatively large α when $\theta_0 > 0$. Figure 2 shows the results of the θ_k dependence of α for three different conditions to produce LIPS Coulomb potentials: LIPS-third ($n_b = 3$), LIPS-fourth ($n_b = 4$), and LIPS-fifth ($n_b = 5$). In spite of the difference of constraint conditions, basis potentials around $\theta_l = 2\pi/5$ provide the smallest α.

Parameters for the determination of LIPS Coulomb potentials are shown in section 2 of Supporting Information. Figure 3 illustrates $\phi^*_{LIPS}(r/2r_c)$ for the three variations of the LIPS Coulombic potential. The coefficient c_k associated with each basis potential can have large values, but the values are just a mathematical consequence and one should not mistake them with physically attributed charges placed in the ambient. The following inequality can be verified by Figure 3. $\phi^*_{LIPS}(r/2r_c)$ has

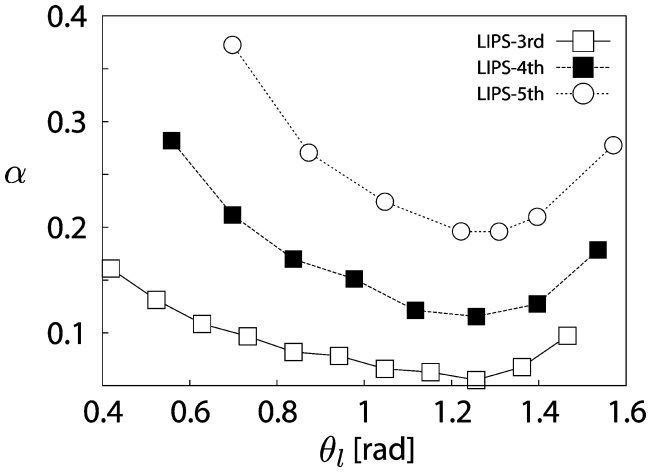

Figure 2. θ_k dependence of α for three different conditions to produce LIPS Coulomb potentials: LIPS-third ($n_b = 3$), LIPS-fourth ($n_b = 4$), and LIPS-fifth ($n_b = 5$). In spite of the difference of constraint conditions, basis potentials around $\theta_l = 2\pi/5$ provide the smallest α.

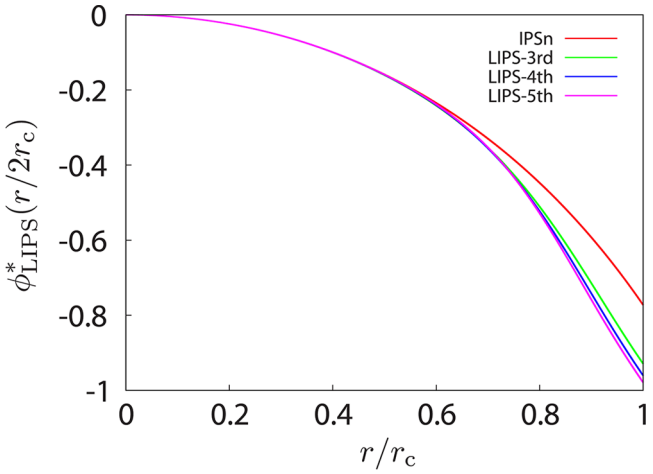

Figure 3. Shape of $\phi^*_{LIPS}(r/2r_c)$ for the three variations of LIPS Coulombic potential: LIPS-third, LIPS-fourth, and LIPS-fifth.

small values (comparable to the values in the axial term of the IPSn method).

$$-1 < \phi^*_{LIPS}(r/2r_c) \leq 0 \tag{13}$$

To explain this, eqs 14 and 15 are derived by non-dimensionalizing and inserting $r = 0$ into eqs 2 and 3, respectively:

$$\sum_{k=1}^{l} c_k\phi^*_k(0, \theta_k) = \left(\sum_{k=1}^{l} c_k\right)\sum_{m=1}^{\infty}\frac{2}{m} \tag{14}$$

$$\phi^*_{random}(0) = \sum_{m=1}^{\infty}(24m^2 + 2)\frac{1}{m} - \left(2\sum_{k=1}^{l} c_k\right)\sum_{m=1}^{\infty}\frac{1}{m} \tag{15}$$

Inserting these two equations in eq 11 gives eq 16:

dx.doi.org/10.1021/ct3003805 | J. Chem. Theory Comput. 2012, 8, 4503−4516

$$\sum_{k=1}^{l} c_k \phi_k^*(r/2r_c, \theta_k) + \phi_{\text{random}}^*(r/2r_c) = \sum_{m=1}^{\infty} (24m^2 + 2)\frac{1}{m} - \phi_{\text{LIPS}}^*(r/2r_c) \quad (16)$$

On the basis of eqs 13 and 16, the following inequality is valid:

$$\sum_{m=1}^{\infty} (24m^2 + 2)\frac{1}{m} \le \sum_{k=1}^{l} c_k \phi_k^*(r/2r_c, \theta_k) + \phi_{\text{random}}^*(r/2r_c) < 1 + \sum_{m=1}^{\infty} (24m^2 + 2)\frac{1}{m} \quad (17)$$

This inequality shows that contributions from the sum of basis potentials and the random term cancel each other out, making them close to the contributions of $\sum_{m=1}^{\infty}(24m^2 + 2)$ image particles. Therefore, the effects from all image particles establish the effects from the $\sum_{m=1}^{\infty}(24m^2 + 2)$ image particles that are identical to the IPSn method (see section 1 of Supporting Information), regardless of the values from c_k values for the particle interactions. This shows that the LIPS method satisfies the density equality between the cutoff region and its surrounding environment. One should realize that only the sum of the anisotropic part ($\sum_{k=1}^{l} c_k \phi_k^*(r/2r_c, \theta_k)$) and isotropic part ($\phi_{\text{random}}^*(r/2r_c)$) of the LIPS method has physical meaning, which is similar in nature to the sum of the decomposition of the anisotropic and isotropic parts for the IPSn method. The axial (anisotropic part) and random image (isotropic part) of the IPSn method themselves individually lack physical meaning compared with their sum. The magnitude of the contribution of each part is determined again merely from the constraint conditions. Therefore, when interactions between i and j particles are considered by the LIPS method, each j particle is affected from the surrounding environment, which is close to the contributions of total $\sum_{m=1}^{\infty}(24m^2 + 2)q$ charges that are isotropically and periodically placed. This fact shows that the actual charge distribution outside the cutoff territory is nearly equal to periodic spherical shells that have a $(24m^2 + 2)q/4\pi(2mr_c)^2$ surface charge density. Again, the images for LIPS calculations are "imaginary", which means they do not explicitly exist in a simulation system and are distributed isotropically and periodically around each particle. This is exactly the same concept as the conventional IPS method.

The form of eq 16 can be changed by use of eq 3, which becomes eq 18:

$$\sum_{k=1}^{l} c_k \left[\sum_{m=1}^{\infty} \int_0^{\pi} \{(r/2r_c)^2 + m^2 - 2m(r/2r_c)\cos\theta\}^{-1/2} \sin\theta \, d\theta - \phi_k^*(r/2r_c, \theta_k) \right] = \sum_{m=1}^{\infty} (24m^2 + 2) \left[\frac{1}{2} \int_0^{\pi} \{(r/2r_c)^2 + m^2 - 2m(r/2r_c)\cos\theta\}^{-1/2} \sin\theta \, d\theta - \frac{1}{m} \right] + \phi_{\text{LIPS}}^*(r/2r_c) \quad (18)$$

Generalizing this by $u(r)$ presents

$$\sum_{k=1}^{l} c_k \left[\sum_{m=1}^{\infty} \int_0^{\pi} u\{(r^2 + 4m^2 r_c^2 - 4mr_c r \cos\theta)^{1/2}\} \sin\theta \, d\theta - \phi_k(r, r_c, \theta_k) \right] = \sum_{m=1}^{\infty} (24m^2 + 2)\frac{1}{2} \int_0^{\pi} u\{(r^2 + 4m^2 r_c^2 - 4mr_c r \cos\theta)^{1/2}\} \sin\theta \, d\theta - \phi_{\text{LIPS}}(r, r_c) \quad (19)$$

Though eq 19 is the sum of the influence of c_k, this is equal to the subtraction of $\phi_{\text{LIPS}}(r,r_c)$ from the sum of effects from the $24m^2 + 2$ particles. In general, when proper boundary conditions for $\phi_{\text{LIPS}}(r,r_c)$ are determined, a physically sound $\phi_{\text{LIPS}}(r,r_c)$ can be constructed, and the potential becomes eq 19. The left-hand side of eq 19 has similar effects from the contributions that the $\sum_{m=1}^{\infty}(24m^2 + 2)$ image particles attribute. Furthermore, at least a double precision of accuracy is required to properly generate $\phi_{\text{LIPS}}(r,r_c)$.

For efficient computation, we present a polynomial even function for LIPS potentials of the Coulombic potential:

$$\phi_{\text{LIPS}}^*(r/2r_c) = \sum_{k_f=1}^{n_f} a_{k_f} (r/r_c)^{2k_f} \quad (20)$$

where n_f is the highest order term of the polynomial function, a_{k_f} are numerical fitting parameters of $\phi_{\text{LIPS}}^*(r/2r_c)$, and $k_f = 1, 2, 3, \ldots, n_f$. Consequently, the numerical function for the LIPS Coulomb potential is expressed by

$$u_{\text{LIPS}}(r, r_c) = \frac{Qq}{4\pi\varepsilon_0} \left\{ \frac{1}{r} + \left(-\frac{1}{2r_c} \right) \sum_{k_f=1}^{n_f} a_{k_f} (r/r_c)^{2k_f} \right\} \quad (21)$$

Numerical fitting parameters for the three variations of LIPS Coulombic potentials are shown in section 3 of Supporting Information. Moreover, the calculation efficiency of the polynomial even function is shown in section 4 of Supporting Information.

2.3. Application of LIPS for Molecular Dynamics Simulations. $u_{\text{LIPS}}(r,r_c)$ has a smooth transition for k_bth order derivatives from the inside to the outside of the cutoff boundary. However, $u_{\text{LIPS}}(r,r_c)$ has a nonzero value on the cutoff boundary in general. To avoid energy discontinuity crossing the boundary, the following form is used for an actual calculation of intermolecular energy in MD simulations:

$$u_{\text{LIPS}}^{\text{inter}}(r, r_c) = \begin{cases} u_{\text{LIPS}}(r, r_c) - u_{\text{LIPS}}(r_c, r_c) & \text{for } r \le r_c \\ 0 & \text{for } r > r_c \end{cases} \quad (22)$$

where $u_{\text{LIPS}}(r_c,r_c)$ is the cutoff boundary energy of the LIPS potential. The total intermolecular energy by use of $u_{\text{LIPS}}^{\text{inter}}(r,r_c)$, $U_{\text{inter}}(r_c)$ is

$$U_{\text{inter}}(r_c) = \frac{1}{2} \sum_i \sum_j u_{\text{LIPS}}^{\text{inter}}(r_{ij}, r_c) \quad (23)$$

Furthermore, the following intramolecular self-energy of covalent bonded atom pairs should be calculated when molecules contain more than one atom:

$$u_{\mathrm{LIPS}}^{\mathrm{intra}}(r, r_c) = \begin{cases} \chi u(r) - u(r_c) + \phi_{\mathrm{LIPS}}(r, r_c) - \phi_{\mathrm{LIPS}}(r_c, r_c) & \text{for } r \le r_c \\ 0 & \text{for } r > r_c \end{cases} \tag{24}$$

where χ is the scaling factor for covalent bonded atom pairs. Normally, χ takes the following form:

$$\chi = \begin{cases} 0 & \text{for } 1-1,\ 1-2,\ \text{and } 1-3 \text{ covalent bonded atom pairs} \\ \chi_{(1-4)} & \text{for } 1-4 \text{ covalent bonded pairs} \\ 1 & \text{otherwise} \end{cases} \tag{25}$$

The total intramolecular self-energy, $U_{\mathrm{intra}}(r_c)$, is expressed by

$$U_{\mathrm{intra}}(r_c) = \frac{1}{2} \sum_{i_{\mathrm{mol}}} \sum_{\kappa} \sum_{\lambda} u_{\mathrm{LIPS}}^{\mathrm{intra}}(r_{\kappa\lambda}, r_c) \tag{26}$$

where i_{mol} is the index of molecules, and both κ and λ are indices of particles within a single molecule.

The total boundary energy, $U_{\mathrm{bound}}(r_c)$, can be expressed by

$$U_{\mathrm{bound}}(r_c) = \frac{1}{2} \sum_{i} \sum_{r_{ij} \le r_c} u_{\mathrm{LIPS}}(r_c, r_c) \tag{27}$$

$$U_{\mathrm{bound}}(r_c) \approx \frac{2\pi {r_c}^3}{3V} \sum_{i} \sum_{j} u_{\mathrm{LIPS}}(r_c, r_c) \tag{28}$$

where V is the volume of the system. Equation 28 is based on a homogeneous approximation.

In consequence, the total energy is expressed by

$$U_{\mathrm{LIPS}}(r_c) = U_{\mathrm{inter}}(r_c) + U_{\mathrm{intra}}(r_c) + U_{\mathrm{bound}}(r_c) \tag{29}$$

3. SIMULATION SYSTEMS AND CONDITIONS

MD simulations for bulk water and water−vapor interfacial systems were conducted to examine the accuracy of the LIPS method for calculating the Coulombic interaction, and physical properties were compared with those from the simulations of IPSn, IPSp, and Ewald sum. In order to clarify the effect of Coulombic interaction for LIPS, IPSn, and IPSp, they were applied only for the Coulombic potential, and a cutoff method was used for the Lennard-Jones (LJ) potential.

This work also requires computational power to simulate many time steps for long cutoff radii, so a special-purpose computer for molecular dynamics, MDGRAPE-3,[60−62] was used.

3.1. Bulk Water. For bulk water simulations, the cutoff radius of the LJ potential was set as 1.2664 nm, which is 4.0 in LJ length units because physical properties of bulk LJ systems have been found to be reasonable when the cutoff radius is larger than 3.0.[53] For the LIPS, IPSn, and IPSp methods, the cutoff radius r_c of the Coulombic potential was changed from 1.2 to 2.8 nm in 0.2 nm increments. The cutoff radius for the real part of the Ewald sum method was set to 2.8 nm for efficient calculations using MDGRAPE-3. In this simulation, the extended simple point charge (SPC/E) model[63] was used for water molecules. The velocity Verlet algorithm[64] was used with three-dimensional periodic boundary conditions along with a time step of 2 fs. The atoms in a water molecule were constrained by the RATTLE algorithm.[65] The simulation was performed in a constant particle number, volume, and temperature ensemble with the Nosé−Hoover thermostat,[66,67] where the number of water molecules was 6192; the density was 0.997 cm^3, and the temperature was 298.15 K. After equilibration of the system, a total of 5×10^5 time steps (1 ns) were carried out for each cutoff radius of the LIPS, IPSn, and IPSp methods. The potential energy, self-diffusion coefficient, radial distribution function, and distance-dependence Kirkwood factor were mainly calculated. We calculated the self-diffusion coefficient D for the transport coefficients. The self-diffusion coefficient can be determined either by the Einstein relationship or by the Green−Kubo formula, which are basically equivalent formulas. Here we used the Einstein relationship:

$$D = \lim_{t \to \infty} \frac{1}{6t} \langle |r_i(t) - r_i(0)| \rangle_N \tag{30}$$

where $r_i(t)$ is the position of particle i, t is the time, and $\langle \cdots \rangle_N$ denotes the particle average. The angular brackets indicate an equilibrium ensemble average, and the slope of the mean-squared displacement of the diffusing particle in the long-time limit is calculated for the diffusion coefficient. The radial distribution function $g(r)$, distance-dependent Kirkwood factor $G_k(r)$, and radial orientation of the dipole $\langle \cos \theta(r) \rangle_e$ were mainly calculated for the configuration of water. These properties are given as a function of the distance between two water molecules, denoted r. The conventional expressions give

$$g(r) = \frac{V}{4\pi r^2 \Delta r N(N-1)} \left\langle \sum_i n_i(r) \right\rangle_e \tag{31}$$

$$G_k(r) = \frac{1}{N} \left\langle \sum_i (u_i \sum_{j, r_{ij} < r} u_j) \right\rangle_e \tag{32}$$

and

$$\langle \cos \theta(r) \rangle_e = \frac{1}{N} \left\langle \sum_i \frac{1}{n_i(r)} \left(\sum_{j=1}^{n_i(r)} u_i u_j \right) \right\rangle_e \tag{33}$$

where $n_i(r)$ is the number of molecules that exist in the region between r and $r + \Delta r$ from molecule i; u_i and u_j are the normalized dipole moments of molecules i and j, respectively; θ is the angle between the dipole moments of two water molecules i and j; and $\langle \cdots \rangle_e$ signifies the ensemble average.

3.2. Water−Vapor Interface. In the simulations of water−vapor interfacial systems, the cutoff radius of the LJ potental was set as 2.5328 nm, which is 8.0 in LJ length units. For the LIPS method, the cutoff radius of the Coulombic potential was changed from 7.0 to 10.5 nm by 1.75 nm increments. Moreover, water was again simulated with the SPC/E model, and all other conditions were the same as the bulk case. The number of water molecules was 10 976, and the temperature was 298.15 K. The sizes of the simulation box for x-, y-, and z-directions were $L_x = 7$ nm, $L_y = 7$ nm, and $L_z = 21$ nm. The x- and y-axes were tangential to the interface, and the z-axis was normal to the interface. After equilibration of the system, a total of 5×10^5 time steps (1 ns) were carried out for each cutoff radius of the LIPS method. The potential energy, surface tension, electric potential profile $\psi(z)$, and dipole orientational function $\langle \rho(z) \cos(\theta) \rangle$ were calculated. The surface tension was evaluated from

dx.doi.org/10.1021/ct3003805 | J. Chem. Theory Comput. 2012, 8, 4503−4516

$$\gamma = 0.5\langle L_z\{P_{zz} - 0.5(P_{xx} + P_{yy})\}\rangle_e \quad (34)$$

where L_z is the size of the simulation box normal to the interface, P_{zz} is the normal component of the internal pressure tensor, and P_{xx} and P_{yy} were the tangential components. Because two interfaces exist, a prefactor of 0.5 was required to obtain γ on a per-interface basis. The electrostatic potential profile of the water−vapor system at the interface was calculated by double integration of the Poisson equation:

$$\psi(z) - \psi(0) = -\frac{4\pi}{\varepsilon_0}\int_0^{\infty}\int_0^{z'}\rho_c(z'')\,dz''\,dz' \quad (35)$$

where ρ_c is the time-averaged charge density. The zero on the left-hand side means vacuum for liquid−vapor systems and the center of the hydrophobic layer for liquid−liquid systems. The dipole orientational function, $\langle\rho(z)\cos(\theta)\rangle_e$, is the orientation of water dipoles with respect to the surface normal (z-axis), which is scaled by the electron density. θ is the angle between the dipole vector and the positive z-axis.

The results are compared to data of IPSn, IPSp, and Ewald sum from our previous study.[57]

4. RESULTS AND DISCUSSION

4.1. Bulk Water. *4.1.1. Potential Energy.* Thermodynamic properties for LIPS, IPSn, IPSp, and Ewald sum methods were calculated by averaged potential energies. Figure 4 shows the

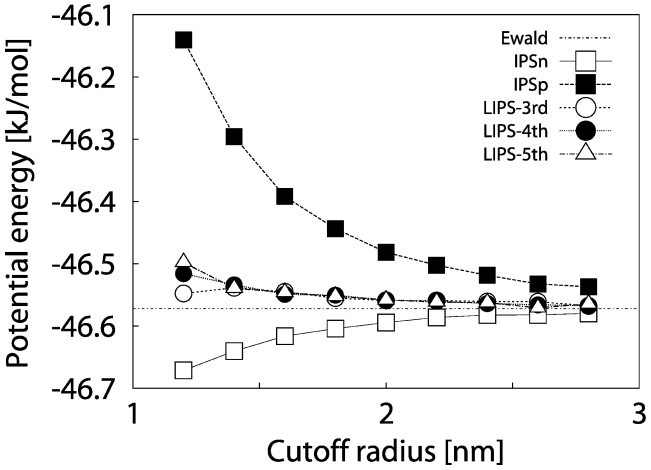

Figure 4. Potential energy of the IPSn, IPSp, LIPS, and Ewald sum methods. All three variations of the LIPS method started to converge at $r_c \geq 2.0$ nm and had the same value as $\langle U_{i,\mathrm{Ewald}}\rangle_e$ (within 0.03%). $\langle U_{i,\mathrm{IPSn}}\rangle_e$ started to converge at $r_c \geq 2.2$ nm and had the same value as $\langle U_{i,\mathrm{Ewald}}\rangle_e$ (within 0.03%). The saturation of potential energy for IPSp was slow in comparison to LIPS and IPSn. $\langle U_{i,\mathrm{IPSp}}\rangle_e$ does not converge at 1.2 nm $\leq r_c \leq$ 2.8 nm.

averaged potential energy per molecule with different cutoff radii for the four methods: $\langle U_{i,\mathrm{LIPS}}\rangle_e$, $\langle U_{i,\mathrm{IPSn}}\rangle_e$, $\langle U_{i,\mathrm{IPSp}}\rangle_e$, and $\langle U_{i,\mathrm{Ewald}}\rangle_e$. All three variations of the LIPS method started to converge at $r_c \geq 2.0$ nm and had the same value as $\langle U_{i,\mathrm{Ewald}}\rangle_e$ within 0.03%. $\langle U_{i,\mathrm{LIPS}}\rangle_e$ has less than 0.02% relative error from $\langle U_{i,\mathrm{Ewald}}\rangle_e$ at $r_c = 2.8$ nm. $\langle U_{i,\mathrm{IPSn}}\rangle_e$ started to converge at $r_c \geq 2.2$ nm and had the same value as $\langle U_{i,\mathrm{Ewald}}\rangle_e$ within 0.03%. $\langle U_{i,\mathrm{IPSn}}\rangle_e$ also has less than 0.02% relative error from $\langle U_{i,\mathrm{Ewald}}\rangle_e$ at $r_c = 2.8$ nm. The saturation of potential energy for IPSp was slow in comparison to LIPS and IPSn. $\langle U_{i,\mathrm{IPSp}}\rangle_e$ does not converge within 1.2 nm $\leq r_c \leq$ 2.8 nm. $\langle U_{i,\mathrm{IPSn}}\rangle_e$ has 0.08% relative error from $\langle U_{i,\mathrm{Ewald}}\rangle_e$ at $r_c = 2.8$ nm.

4.1.2. Self-Diffusion Coefficient. We calculated the self-diffusion coefficients for the LIPS, IPSn, IPSp, and Ewald sum methods for the transport properties. The self-diffusion coefficient D was estimated from the slope of the mean square displacement, $\langle|r_i(t) - r_i(0)|\rangle_N$ in eq 30. For LIPS, IPSn, IPSp, and Ewald sum, the mean square displacement is clearly a linear function with time, and the self-diffusion coefficient can be estimated by the slope. Figure 5 shows the self-diffusion

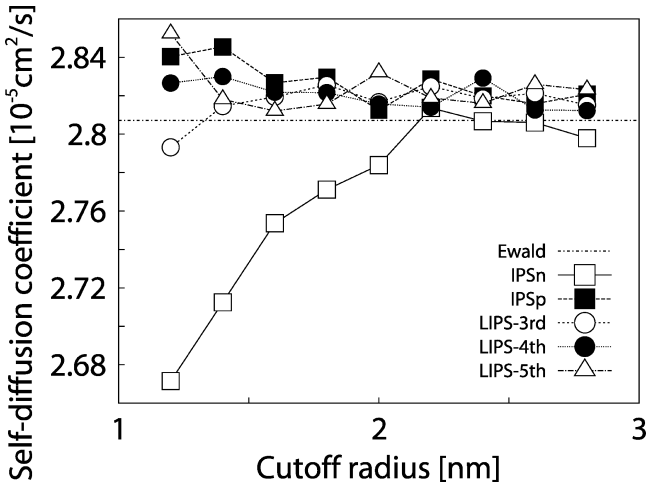

Figure 5. Self-diffusion coefficients of the IPSn, IPSp, LIPS, and Ewald sum methods. For all three variations of LIPS and IPSp, the self-diffusion coefficient is saturated at $r_c \geq 1.6$ nm, and the saturated value of D_{LIPS} and D_{IPSp} is almost the same as D_{Ewald} (within 0.9%). For the IPSn method, the self-diffusion coefficient starts to saturate at $r_c \geq 2.0$ and has the same value as D_{Ewald} (within 0.9%).

coefficients for the four methods: D_{LIPS}, D_{IPSn}, D_{IPSp}, and D_{Ewald}. For all three variations of LIPS and IPSp, the self-diffusion coefficient is saturated at $r_c \geq 1.6$ nm, and the saturated value of D_{LIPS} and D_{IPSp} is almost the same as D_{Ewald} (within 0.9%). For the IPSn method, the self-diffusion coefficient started to saturate at $r_c \geq 2.0$ and had the same value as D_{Ewald} (within 0.9%).

4.1.3. Radial Distribution Functions. To examine the structure around a molecule for the LIPS, IPSn, and IPSp methods, radial distribution functions (RDF) was calculated. Figure 6 shows the oxygen−oxygen RDF of the water molecule for IPSn, IPSp, and three variations of the LIPS method—$g_{\mathrm{OO,IPSn}}(r)$, $g_{\mathrm{OO,IPSp}}(r)$, $g_{\mathrm{OO,LIPS\text{-}third}}(r)$, $g_{\mathrm{OO,LIPS\text{-}fourth}}(r)$, and $g_{\mathrm{OO,LIPS\text{-}fifth}}(r)$—at $r_c = 2.2$ nm (Figure 6a) and at $r_c = 2.8$ nm (Figure 6b), and $g_{\mathrm{OO,Ewald}}(r)$, which is for the Ewald sum. In both panels of Figure 6, $g_{\mathrm{OO,IPSn}}(r)$ has a notable deviation from those of the Ewald sum. On the other hand, the estimation of the RDF is dramatically improved by LIPS. Figure 6a shows that the deviation of $g_{\mathrm{OO,LIPS\text{-}fourth}}(r)$ and $g_{\mathrm{OO,LIPS\text{-}fifth}}(r)$ started to converge and provided adequate accuracy. In the case of Figure 6b, $g_{\mathrm{OO,LIPS\text{-}fourth}}(r)$ and $g_{\mathrm{OO,LIPS\text{-}fifth}}(r)$ are almost the same as $g_{\mathrm{OO,Ewald}}(r)$, and the deviation of $g_{\mathrm{OO,LIPS\text{-}third}}(r)$ started to converge. The RDF of oxygen−hydrogen and hydrogen−hydrogen have very similar behavior in comparison to oxygen−oxygen in Figure 6.

To examine the decrease of the deviation for r_c thoroughly, we plotted the root-mean-square deviation (rmsd) of the oxygen−oxygen RDF for IPSn, IPSp, and LIPS methods against

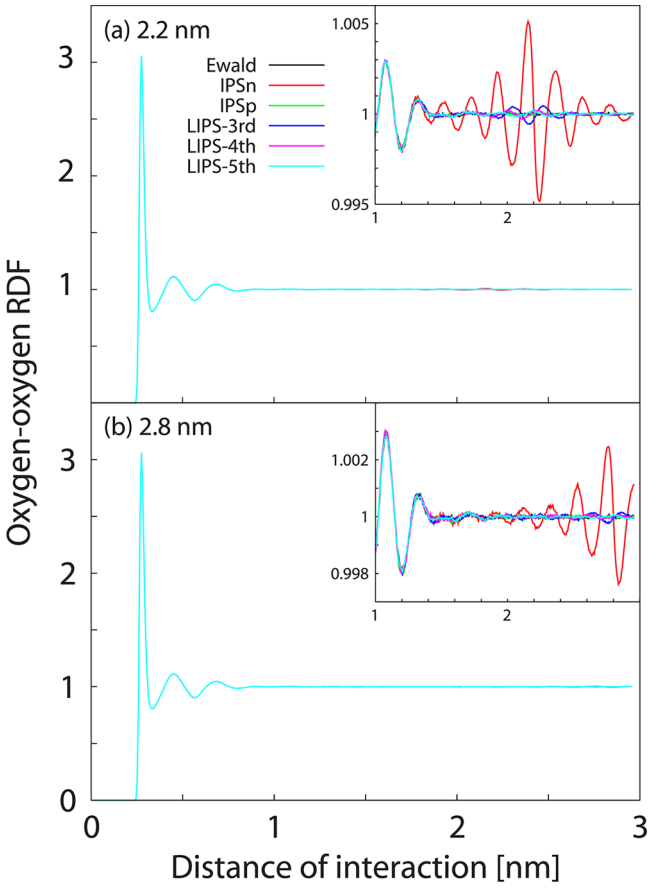

Figure 6. Oxygen−oxygen RDF of the SPC/E water molecule for IPSn, IPSp, LIPS, and Ewald sum methods at (a) r_c = 2.2 nm and (b) r_c = 2.8 nm. In both panels, $g_{OO,IPSn}(r)$ have notable deviations from those of the Ewald sum. On the other hand, the estimation of the RDF is dramatically improved by LIPS. The deviation of $g_{OO,LIPS\text{-}fourth}(r)$ and $g_{OO,LIPS\text{-}fifth}(r)$ started to converge and provided adequate accuracy at r_c = 2.2 nm (panel a). Furthermore, $g_{OO,LIPS\text{-}fourth}(r)$ and $g_{OO,LIPS\text{-}fifth}(r)$ are almost the same as $g_{OO,Ewald}(r)$, and the deviation of $g_{OO,LIPS-third}(r)$ start to converge at r_c = 2.8 nm (panel b). The oxygen−hydrogen and hydrogen−hydrogen RDF have very similar behavior to the oxygen−oxygen RDF.

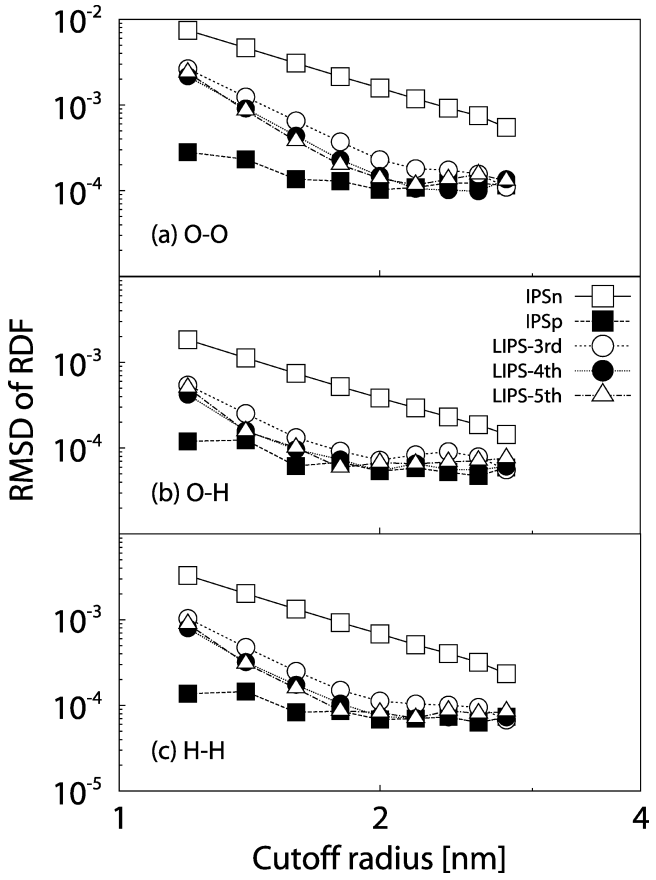

Figure 7. Root-mean-square deviations of (a) oxygen−oxygen, (b) oxygen−hydrogen, and (c) hydrogen−hydrogen RDF for IPSn, IPSp, and LIPS methods vs Ewald sum at different cutoff radii. The rmsd of IPSn decreases roughly in proportion to r_c^{-3}. The rmsd of LIPS has a tendency against cutoff radius like that of IPSn, but a faster decline is achieved. Root-mean-square deviations of $g_{LIPS-third}(r)$, $g_{LIPS-fourth}(r)$, and $g_{LIPS-fifth}(r)$ decrease roughly in proportion to r_c^{-5}, $r_c^{-5.5}$, and r_c^{-6}, respectively. Furthermore, rmsd of $g_{LIPS\text{-}fourth}(r)$ and $g_{LIPS\text{-}fifth}(r)$ converge at $r_c \geq 2.0$ nm, and that of $g_{LIPS\text{-}third}(r)$ starts to converge $r_c \geq 2.2$ nm. The converged values of rmsd for all three variations of LIPS have almost the same value as that of IPSp.

the Ewald sum at different cutoff radii in Figure 7a. Root-mean-square deviations of the oxygen−hydrogen and hydrogen−hydrogen RDF are also plotted in Figure 7 panels b and c, respectively. In the case of IPSn, rmsd decreases roughly in proportion to r_c^{-3}. This means that some extensive properties calculated by IPSn have a commeasurable error to r_c^{-1}. The spatial distribution of water molecules is one of them. The distribution of number of water molecules, $\langle n(r)\rangle_e$, is evaluated by

$$\langle n(r)\rangle_e \approx 4\pi\rho r^2 g(r)\Delta r \tag{36}$$

where r is the distance from any water molecule and $\Delta r \ll r$. Now we focus on the range around $r = r_c$, $r_c - (\Delta r/2) < r < r_c + (\Delta r/2)$. In this range, $g(r) \approx 1$ is assumed for ordinal $g(r)$ for simplicity. $g_{IPSn}(r)$ has $\pm\,\delta/r_c^3$ error, so $g(r) \approx 1 \pm \delta/r_c^3$ can be assumed. An absolute error of the number of water molecules around $r = r_c$ for IPSn, $|\langle n(r_c)\rangle_{e,IPSn} - \langle n(r_c)\rangle_{e,Ewald}|$, is evaluated with

$$|\langle n(r_c)\rangle_{e,IPSn} - \langle n(r_c)\rangle_{e,Ewald}| = 4\pi\rho r_c^2 \Delta r \frac{\delta}{r_c^3} = \frac{4\pi\rho\Delta r\delta}{r_c} \tag{37}$$

This slow decrease in error means that IPSn requires a long cutoff radius for adequate estimation of some extensive properties. On the other hand, rmsd of IPSp has an adequate accuracy in any cutoff radius. The countercharge assumption for polar molecular systems works better for bulk water systems. The rmsd of LIPS has a similar tendency with IPSn for cutoff radii, but a faster decline is observed. Root-mean-square deviations of $g_{LIPS\text{-}third}(r)$, $g_{LIPS\text{-}fourth}(r)$, and $g_{LIPS\text{-}fifth}(r)$ decrease roughly in proportion to r_c^{-5}, $r_c^{-5.5}$, and r_c^{-6}, respectively. Cutoff boundary conditions for higher derivatives of LIPS potentials are better for bulk water systems, and an increase in the number of boundary conditions provides faster convergence of intensive and extensive properties of the spatial distribution of molecules against the cutoff radius. Furthermore, LIPS gives accurate estimations of these properties. Root-mean-square deviations of $g_{LIPS\text{-}fourth}(r)$ and $g_{LIPS\text{-}fifth}(r)$ converge at $r_c \geq 2.0$ nm, and that of $g_{LIPS\text{-}third}(r)$ starts to converge for $r_c \geq 2.2$

dx.doi.org/10.1021/ct3003805 | J. Chem. Theory Comput. 2012, 8, 4503−4516

nm. Converged values of rmsd for all three variations of LIPS have almost the same value as that of IPSp.

4.1.4. Dipole−Dipole Correlation. We focused on the distance-dependence Kirkwood factor, $G_k(r)$, where one can see the dipole−dipole correlation of bulk water systems. $G_k(r)$ has a strong cutoff radius effect, and the influence of the interaction treatment is quantitatively expressible by the shape of $G_k(r)$. An evident shortcoming of the cutoff-like method appears for the $G_k(r)$ value in bulk water systems. Thus, the distance dependence of the Kirkwood factors $G_{k,\mathrm{IPSn}}(r)$, $G_{k,\mathrm{IPSp}}(r)$, $G_{k,\mathrm{LIPS\text{-}third}}(r)$, $G_{k,\mathrm{LIPS\text{-}fourth}}(r)$, $G_{k,\mathrm{LIPS\text{-}fifth}}(r)$, and $G_{k,\mathrm{Ewald}}(r)$ of the various cutoff radii were calculated to evaluate the cutoff radius effect of the dipole−dipole correlation.

Figure 8 shows the shape of $G_{k,\mathrm{IPSn}}(r)$, $G_{k,\mathrm{IPSp}}(r)$, $G_{k,\mathrm{LIPS\text{-}third}}(r)$, $G_{k,\mathrm{LIPS\text{-}fourth}}(r)$, $G_{k,\mathrm{LIPS\text{-}fifth}}(r)$, and $G_{k,\mathrm{Ewald}}(r)$. It is clearly seen that $G_{k,\ \mathrm{IPSn}}(r)$ fluctuates near r_c as in $g_{\mathrm{IPSn}}(r)$, and this fluctuation still remains in spite of the increment of the cutoff radius. $G_k(r)$ is an extensive property, so IPSn has an absolute error, which is proportional to r_c^{-1} on some extensive properties. Therefore, the decrease of $G_{k,\mathrm{IPSn}}(r)$ fluctuation against the increment of the cutoff radius is slow. The artificial configuration in $G_k(r)$ of IPSn is not seen in IPSp nor in LIPS variations. IPSp and LIPS can estimate $G_k(r)$ more adequately than IPSn.

The result of $\langle\cos\theta(r)\rangle_e$ shows the radial distribution for orientation of the water dipole moment. Figure 9 presents $\langle\cos\theta(r)\rangle_{e,\mathrm{IPSn}}$, $\langle\cos\theta(r)\rangle_{e,\mathrm{IPSp}}$, $\langle\cos\theta(r)\rangle_{e,\mathrm{LIPS\text{-}third}}$, $\langle\cos\theta(r)\rangle_{e,\mathrm{LIPS\text{-}fourth}}$, and $\langle\cos\theta(r)\rangle_{e,\mathrm{LIPS\text{-}fifth}}$ at r_c = 2.2 nm; $\langle\cos\theta(r)\rangle_{e,\mathrm{Ewald}}$, is also plotted for comparison. $\langle\cos\theta(r)\rangle_{e,\mathrm{IPSn}}$ still fluctuates near r_c as in $g_{\mathrm{IPSn}}(r)$ in spite of the long cutoff radius. $\langle\cos\theta(r)\rangle_e$ is connected with $g(r)$ and $G_k(r)$ by the following equation:

$$\langle\cos\theta(r)\rangle_e = \frac{V}{4\pi r^2(N-1)g(r)}\frac{\partial G_k(r)}{\partial r} \tag{38}$$

In spite of this relationship, the deviation of $\langle\cos\theta(r)\rangle_{e,\mathrm{IPSn}}$ is not canceled out by the deviation of $g(r)$ and $G_k(r)$. This shows that the cause of deviation of $\langle\cos\theta(r)\rangle_{e,\mathrm{IPSn}}$ is not only an anomalous spatial distribution of water molecules calculated by IPSn but also a multipole effect, which is evaluated by IPSn. The cutoff boundary condition for IPSn gives poor estimation of the multipole effect around r_c. Since the multipole effect of water molecular systems is strong, the deviation of $\langle\cos\theta(r)\rangle_{e,\mathrm{IPSn}}$ due to the cutoff boundary condition of IPSn seems to become apparent. There are no singular configurations of $\langle\cos\theta(r)\rangle_e$ like IPSn in the case of IPSp and all three LIPS variations. The artificial configuration of $G_k(r)$ like IPSn is not seen in IPSp and all three LIPS variations. IPSp and LIPS give adequate accuracy for estimating $\langle\cos\theta(r)\rangle_e$.

To display the cutoff radius tendency of the deviation, rmsd of $\langle\cos\theta(r)\rangle_{e,\mathrm{IPSn}}$, $\langle\cos\theta(r)\rangle_{e,\mathrm{IPSp}}$, $\langle\cos\theta(r)\rangle_{e,\mathrm{LIPS\text{-}third}}$, $\langle\cos\theta(r)\rangle_{e,\mathrm{LIPS\text{-}fourth}}$, and $\langle\cos\theta(r)\rangle_{e,\mathrm{LIPS\text{-}fifth}}$ from $\langle\cos\theta(r)\rangle_{e,\mathrm{Ewald}}$ at different cutoff radii in Figure 10 were plotted. The results of rmsd for IPSn, IPSp, and three variations of LIPS were less than 10^{-3} in 1.2 nm $\leq r_c \leq$ 2.8 nm. All IPS techniques give adequate estimations for $\langle\cos\theta(r)\rangle_e$, but the cutoff radius tendency is different. Root-mean-square deviations of IPSp, LIPS-fourth, and LIPS-fifth gradually decrease by a cutoff radius increment and converge around 10^{-4} in $r_c \geq$ 2.2 nm. On the other hand, rmsd of IPSn and LIPS-third do not have a definite tendency against changes of the cutoff radius.

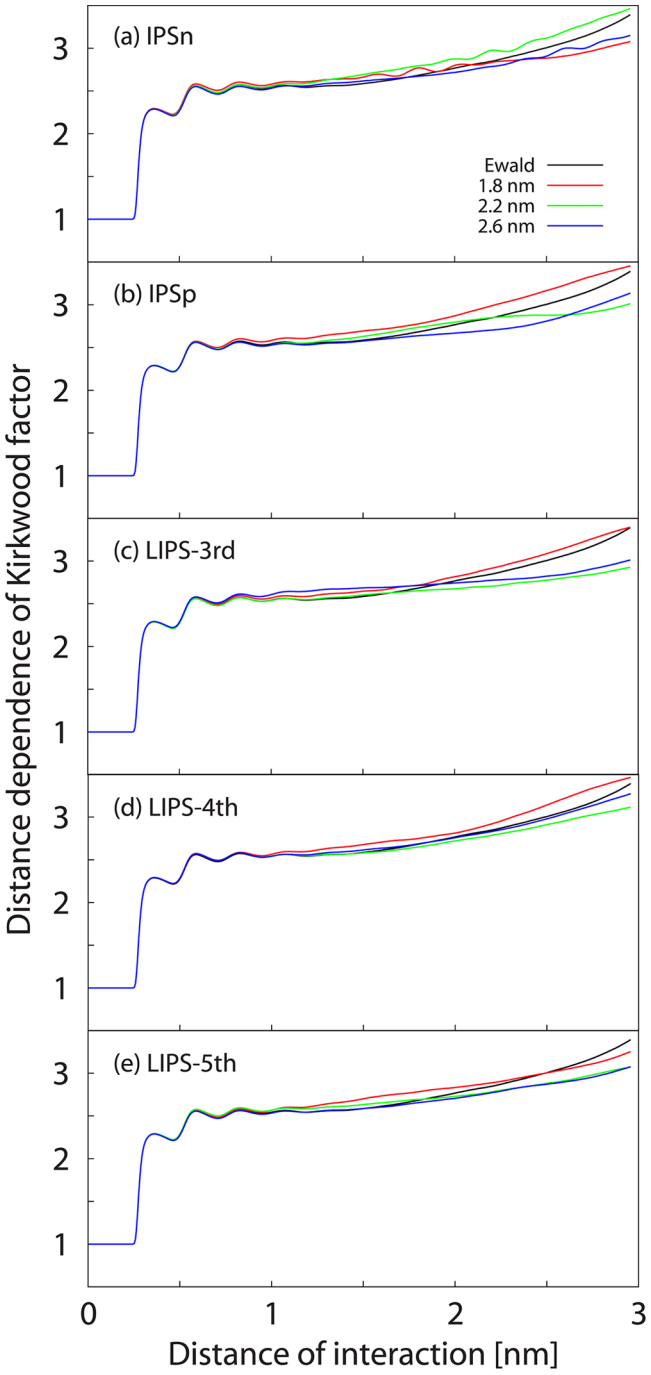

Figure 8. Distance-dependence Kirkwood factors for IPSn, IPSp, LIPS, and Ewald sum methods. It is clearly seen that $G_{k,\mathrm{IPSn}}(r)$ fluctuates near r_c as in $g_{\mathrm{IPSn}}(r)$, and this fluctuation still remains in spite of the increment of the cutoff radius. $G_k(r)$ is one of the extensive properties, and IPSn imposes an absolute error, which is proportional to r_c^{-1} on some extensive properties. Therefore, the decrease of $G_{k,\mathrm{IPSn}}(r)$ fluctuation against the increment of the cutoff radius is slow. The artificial configuration of $G_k(r)$ like IPSn is not seen in IPSp and all three LIPS variations. IPSp and LIPS can estimate $G_k(r)$ more adequately than IPSn.

Other additional results for the dipole−dipole correlation of bulk water systems are shown in section 5 of Supporting Information.

4.2. Water−Vapor Interface. *4.2.1. Potential Energy and Surface Tension.* To assess the accuracy in estimating

dx.doi.org/10.1021/ct3003805 | J. Chem. Theory Comput. 2012, 8, 4503−4516

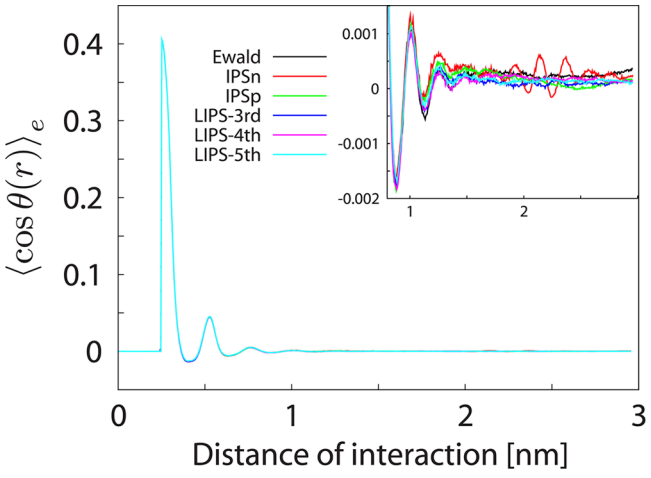

Figure 9. $\langle \cos\theta(r)\rangle_e$ for IPSn, IPSp, LIPS, and Ewald sum methods. $\langle \cos\theta(r)\rangle_{e,IPSn}$ still fluctuates near r_c as in $g_{IPSn}(r)$ in spite of the long cutoff radius. The cutoff boundary condition for IPSn imposes poor estimation of multipole effects around r_c. Since the multipole effect of water molecular systems is strong, the deviation of $\langle \cos\theta(r)\rangle_{e,IPSn}$ due to the cutoff boundary condition of IPSn seems to clearly appear. There are no singular configurations of $\langle \cos\theta(r)\rangle_e$ like IPSn in the case of IPSp and all three LIPS variations. The artificial configuration of $G_k(r)$ like IPSn is not seen in IPSp and all three LIPS variations. IPSp and LIPS give adequate accuracy for estimation of $\langle \cos\theta(r)\rangle_e$.

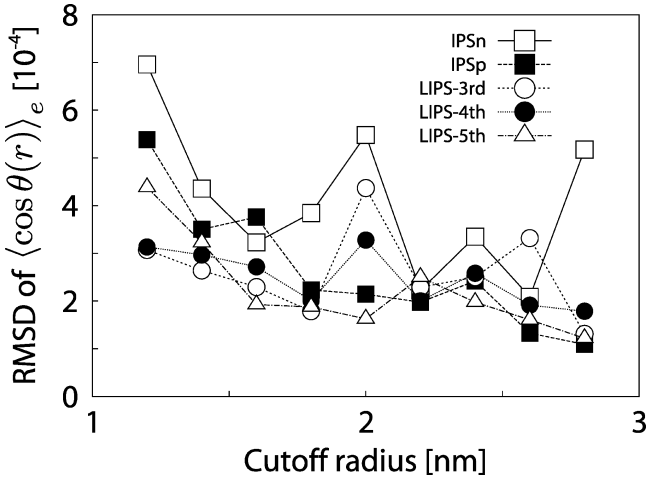

Figure 10. Root-mean-square deviations of $\langle \cos\theta(r)\rangle_e$ for IPSn, IPSp, and LIPS methods against Ewald sum at different cutoff radii. The results of rmsd for IPSn, IPSp, and three variations of LIPS are less than 10^{-3} in 1.2 nm $\leq r_c \leq$ 2.8 nm. All IPS techniques give adequate estimation for $\langle \cos\theta(r)\rangle_e$, but the cutoff radius tendency is different. rmsd of IPSp, LIPS-fourth, and LIPS-fifth gradually decrease by a cutoff radius increment and converge around 10^{-4} in $r_c \geq$ 2.2 nm. On the other hand, rmsd of IPSn and LIPS-third do not have a definite tendency against changes of the cutoff radius.

fundamental thermodynamic properties, potential energy and surface tension for the three variations of LIPS method were calculated. The results of the three variations of LIPS (this work) and IPSn, IPSp and Ewald sum (our previous study)[57] are shown in Table 1.

The potential energy for three variations of LIPS converged for 7.0 nm $\leq r_c \leq$ 10.5 nm and had the same value as that of the Ewald sum within 0.006%. IPSn and IPSp have almost the same accuracy for 7.0 nm $\leq r_c \leq$ 10.5 nm. All IPS techniques give adequate accuracy for estimating the potential energy of water−vapor interfacial systems. Surface tension for the three variations of LIPS at 7.0 nm $\leq r_c \leq$ 10.5 nm had similar values to that of the Ewald sum, which was within 2%. All variations of the LIPS method had adequate accuracy in estimating the surface tension.

Table 1. Potential Energy and Surface Tension for IPSn, IPSp, LIPS, and Ewald Sum Methods[a]

r_c (nm)	potential energy (kJ/mol)	surface tension (mN/m)
	LIPS-third	
7.0	−45.9834(0.0015)	58.63(0.78)
8.75	−45.9799(0.0014)	59.63(0.79)
10.5	−45.9802(0.0015)	58.78(0.79)
	LIPS-fourth	
7.0	−45.9832(0.0015)	57.75(0.77)
8.75	−45.9790(0.0015)	59.65(0.76)
10.5	−45.9802(0.0015)	58.67(0.79)
	LIPS-fifth	
7.0	−45.9807(0.0016)	59.50(0.82)
8.75	−45.9817(0.0014)	58.61(0.75)
10.5	−45.9825(0.0016)	58.80(0.82)
	IPSn	
3.5	−45.9879(0.0015)	57.13(0.77)
5.25	−45.9827(0.0015)	57.86(0.76)
7.0	−45.9836(0.0016)	90.45(0.80)
8.75	−45.9843(0.0015)	58.35(0.76)
10.5	−45.9827(0.0016)	59.15(0.82)
	IPSp	
3.5	−45.9647(0.0015)	57.86(0.78)
5.25	−45.9789(0.0015)	57.16(0.77)
7.0	−45.9801(0.0015)	58.02(0.79)
8.75	−45.9815(0.0015)	58.96(0.77)
10.5	−45.9826(0.0016)	57.16(0.80)
	Ewald sum	
	−45.9810(0.0015)	59.74(0.79)

[a]The results of IPSn, IPSp, and Ewald sum are shown in our previous study.[57] The potential energy of LIPS converged within 7.0 nm $\leq r_c \leq$ 10.5 nm and had a nearly identical value to that of the Ewald sum, which was within 0.006%. The surface tension for LIPS had similar values to that of the Ewald sum within 2% for 7.0 nm $\leq r_c \leq$ 10.5 nm. All three variations of LIPS have adequate accuracy to estimate the potential energy and surface tension of water−vapor interfacial systems.

Previous studies found IPSn to produce an abnormal deviation for the surface tension at $r_c = L_z/3 = 7.0$ nm, whereas IPSp and LIPS give sound accuracy. The reason is related to the difference in treatment of the cutoff boundary between IPSn and other IPS techniques. In the case of $r_c = L_z/3 = 7.0$ nm, the cutoff boundary is on the water surface, but all IPS techniques require the bulk structure to be around the cutoff boundary. In spite of this fact, the value of the surface tension strongly deviates only when IPSn is applied. IPSp and LIPS have cutoff boundary conditions for multipoles, whereas IPSn has only one cutoff boundary condition for nonpolar charges. Water molecules on the surface (cutoff boundary) are affected by the discontinuous energy barrier of the IPSn potential and become the source of the eccentric deviation of the surface tension.

4.2.2. Water Configuration. To examine the electrostatic structure of the water surface and slab for the LIPS method, the electrostatic potential profile was calculated. $\psi(z)$ is very sensitive to the cutoff radius, so a difference of electrostatic configuration from other methods can be easily observed.

dx.doi.org/10.1021/ct3003805 | J. Chem. Theory Comput. 2012, 8, 4503−4516

Figure 11 shows the $\psi_{IPSn}(z)$, $\psi_{IPSp}(z)$, $\psi_{LIPS\text{-}third}(z)$, $\psi_{LIPS\text{-}fourth}(z)$, and $\psi_{LIPS\text{-}fifth}(z)$ at r_c = 7.0 nm (Figure 11a), at

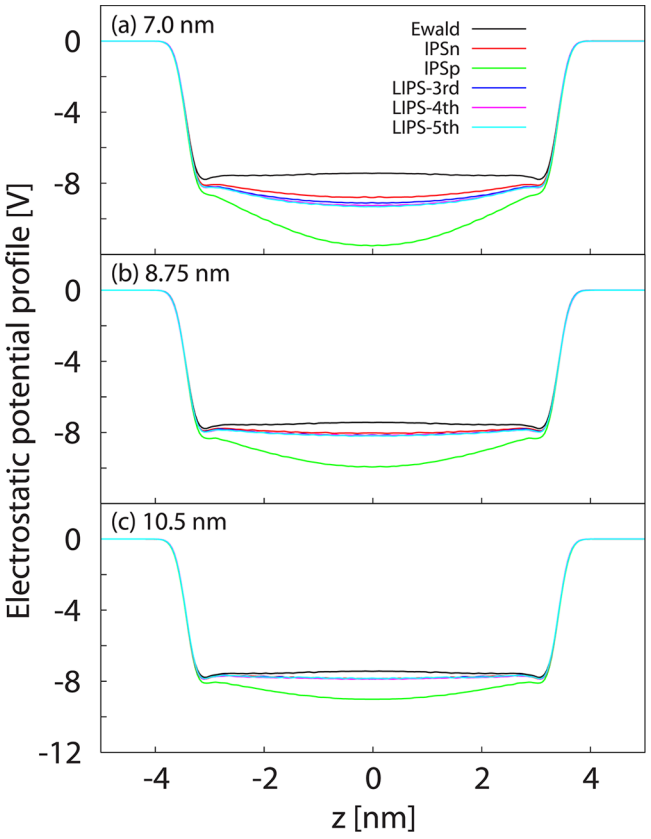

Figure 11. Electrostatic potential profile for IPSn, IPSp, and LIPS methods at (a) r_c = 7.0 nm, (b) r_c = 8.75 nm, and (c) r_c = 10.5 nm and for the Ewald sum method. The accuracy of LIPS is much better in comparison with that of IPSp. Furthermore, the accuracy of LIPS is almost the same as that of IPSn, which is the most accurate method for estimation of electrostatic structure.[57] The shape of the $\psi(z)$ from all three variations of LIPS is almost the same as that of IPSn at 7.0 nm ≤ r_c ≤ 10.5 nm. $\psi(z)$ of a water slab seems to be flat in the case of LIPS and IPSn with r_c = 10.5 nm, and the deviation from that of the Ewald sum is the smallest.

r_c = 8.75 nm (Figure 11b), and at r_c = 10.5 nm (Figure 11c) and also shows $\psi_{Ewald}(z)$, which is for the Ewald sum. As is evident in Figure 11, the accuracy of LIPS is much better in comparison with that of IPSp. Furthermore, the accuracy of LIPS is almost the same as that of IPSn, which is the more accurate IPS method for estimating electrostatic structures.[57] The shape of $\psi(z)$ from all three variations of LIPS is almost the same as that of IPSn at 7.0 nm ≤ r_c ≤ 10.5 nm. $\psi(z)$ of a water slab seems to be flat in the case of LIPS and IPSn with r_c = 10.5 nm, and the deviation from that of the Ewald sum is the smallest.

We also studied the dipole orientational function $\langle\rho(z)\cos(\theta)\rangle_e$, which is another property sensitive to the cutoff radius, so the influence can be quantitatively expressible like the electrostatic potential profile. A crucial shortcoming of the cutoff-like method appears for the $\langle\rho(z)\cos(\theta)\rangle_e$ value in a water−vapor interfacial system. Thus, $\langle\rho(z)\cos(\theta)\rangle_e$ for the LIPS method of various cutoff radii were calculated to understand the influence of the electrostatic structure. To clearly display the discrepancy of $\langle\rho(z)\cos(\theta)\rangle_e$ for the LIPS method from other methods, $\langle\rho(z)\cos(\theta)\rangle_e$ at different cutoff radii were integrated along the z-axis and plotted in Figure 12. The convergence of $\langle\rho(z)\cos(\theta)\rangle_e$ for IPSp is slow in

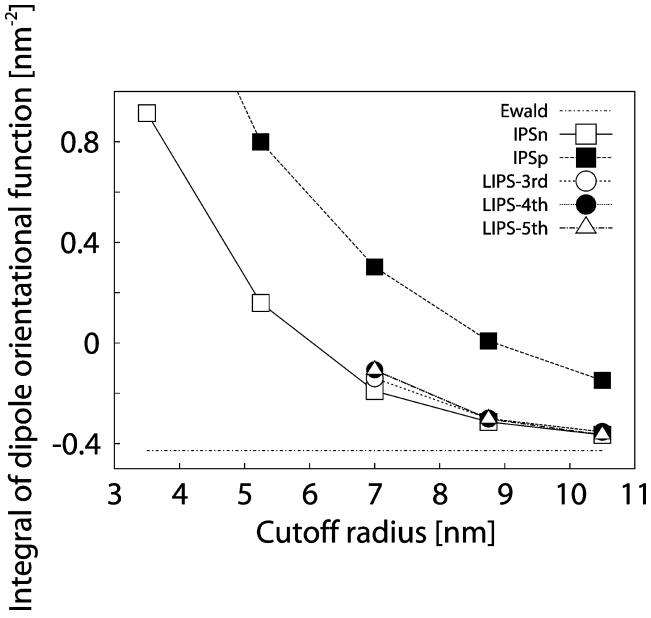

Figure 12. Integral value of $\langle\rho(z)\cos(\theta)\rangle_e$ for IPSn, IPSp, LIPS, and Ewald sum methods at different cutoff radii. The LIPS method has almost the same accuracy as IPSn for the estimation of $\langle\rho(z)\cos(\theta)\rangle_e$ at 7.0 nm ≤ r_c ≤ 10.5 nm. Furthermore, differences of $\langle\rho(z)\cos(\theta)\rangle_e$ from that of the Ewald sum are smallest for LIPS and IPSn at r_c = 10.5 nm.

comparison to that for LIPS and IPSn, and the LIPS method has almost the same accuracy as IPSn for estimating $\langle\rho(z)\cos(\theta)\rangle_e$ at 7.0 nm ≤ r_c ≤ 10.5 nm. Furthermore, differences of $\langle\rho(z)\cos(\theta)\rangle_e$ from that of the Ewald sum are smallest for LIPS and IPSn at r_c = 10.5 nm.

There are two main factors in estimating the electrostatic configuration of cutoff-like methods. One is the length of the cutoff radius. A cutoff radius long enough to cover the interface thickness is required to evaluate the electrostatic configuration. The other factor is the accuracy of the interaction on the water surface. In the IPSp method, it is assumed that there are countercharges around a certain point charge even if the point charge is on the surface. However, the point charge on the surface does not have a countercharge in the direction of the vapor phase. This is why the IPSp method has an inferior result in comparison with LIPS and IPSn for prediction of surface structure.

5. CONCLUSION

In order to make the IPS technique ubiquitous for homogeneous and heterogeneous systems, we developed the LIPS method, which is an improved IPS method using the linear combination of basis potentials. We performed MD simulations on bulk water and water−vapor interfacial systems to evaluate the accuracy of the LIPS method.

For bulk water systems, IPSp has superior accuracy compared with IPSn, but because the former uses countercharges for long-range interactions, it is difficult to use for interfacial systems. The convergence of interfacial properties of the IPSp method is slower than that of the IPSn method. IPSn, on the other hand, has better accuracy for interfacial systems when compared with IPSp, but an atypical spike in the surface

dx.doi.org/10.1021/ct3003805 | J. Chem. Theory Comput. 2012, 8, 4503−4516

tension occurs at certain cutoff radii. Furthermore IPSn cannot properly estimate bulk water systems, since a strong cutoff radius effect for the water configuration occurs. The LIPS method can be used for both systems without loss of accuracy. LIPS-fourth and -fifth at $r_c \geq 2.2$ nm give essentially the same results as the IPSp method in bulk water systems without the countercharge assumption. In interfacial systems, LIPS does not breed an eccentric deviation for the surface tension. All three variations (third, fourth, and fifth) of the LIPS method provide equivalent results as the IPSn method at 7.0 nm $\leq r_c \leq$ 10.5 nm.

The versatility of LIPS is not limited to the type of system in which it can be applied, for it can be coupled with various kinds of potential functions that contain long-range interactions. For further studies, we point out two main discussion points. One is in the choice of constraint conditions and basis potentials. For instance, different types of cutoff-like methods such as the cutoff method that uses switching or shifting functions can be modeled. The LIPS method also has the potential to express many other kinds of force fields, where LIPS-third, -fourth, and -fifth are only some examples of the LIPS method. More suitable constraint conditions for other systems may exist.

The other discussion point is the long cutoff problem. To estimate a surface structure, the LIPS method requires a long cutoff radius like IPSn. For IPS techniques with a long cutoff, Wu and Brooks[51] developed IPS/DFFT, which is a combination of the IPS method and FFT. We have also developed IPS/Tree,[59] which is a combination of the IPS method and the hierarchical tree structure. These methods can be easily combined with the LIPS method.

■ ASSOCIATED CONTENT

Ⓢ Supporting Information

Additional text, 16 equations, one figure, and three tables providing explanation of the conventional IPS method, parameters for determination of Coulombic potential from extended IPS theory, calculation efficiency of polynomial function for the LIPS method, numerical fitting parameters for three variations of LIPS Coulombic potentials, and more additional results of bulk water systems. This material is available free of charge via the Internet at http://pubs.acs.org/.

■ AUTHOR INFORMATION

Corresponding Author

*E-mail takahashi@mech.keio.ac.jp.

Notes

The authors declare no competing financial interest.

■ ACKNOWLEDGMENTS

We sincerely thank Dr. Rio Yokota from King Abdullah University of Science and Technology (KAUST) for fruitful discussions on leading-edge techniques of the tree-based method. K.Z.T. was supported by Grant-in-Aid for Japan Society for the Promotion of Science (JSPS) Fellows 21-5452 of the Ministry of Education, Culture, Sports, Science and Technology (MEXT). T.N. and K.Y. were supported by the Core Research for the Evolution Science and Technology (CREST) of the Japan Science and Technology Corporation (JST). D.S. was supported in part by the Global Center of Excellence Program for "Center for Education and Research of Symbiotic, Safe and Secure System Design" from MEXT.

■ REFERENCES

(1) Hoheisel, C. *J. Chem. Phys.* **1987**, *86*, 2328.
(2) Hoheisel, C.; Vogelsang, R.; Schoen, M. *J. Chem. Phys.* **1987**, *87*, 7195.
(3) Smit, B. *J. Chem. Phys.* **1992**, *96*, 8639−8640.
(4) Trokhymchuk, A.; Alejandre, J. *J. Chem. Phys.* **1999**, *111*, 8510.
(5) Lopez-Lemus, J.; Alejandre, J. *Mol. Phys.* **2002**, *100*, 2983−2992.
(6) Neumann, M.; Steinhauser, O. *Mol. Phys.* **1980**, *39*, 437−454.
(7) Alper, H.; Levy, R. *J. Chem. Phys.* **1989**, *91*, 1242.
(8) Kitchen, D.; Hirata, F.; Westbrook, J.; Levy, R.; Kofke, D.; Yarmush, M. *J. Comput. Chem.* **1990**, *11*, 1169−1180.
(9) Tasaki, K.; McDonald, S.; Brady, J. *J. Comput. Chem.* **1993**, *14*, 278−284.
(10) Smith, P.; van Gunsteren, W. *J. Chem. Phys.* **1994**, *100*, 3169.
(11) Feller, S.; Pastor, R.; Rojnuckarin, A.; Bogusz, S.; Brooks, B. *J. Phys. Chem.* **1996**, *100*, 17011−17020.
(12) van der Spoel, D.; van Maaren, P.; Berendsen, H. *J. Chem. Phys.* **1998**, *108*, 10220.
(13) Mark, P.; Nilsson, L. *J. Comput. Chem.* **2002**, *23*, 1211−1219.
(14) Yonetani, Y. *Chem. Phys. Lett.* **2005**, *406*, 49−53.
(15) van der Spoel, D.; van Maaren, P. *J. Chem. Theory Comput.* **2006**, *2*, 1−11.
(16) Yonetani, Y. *J. Chem. Phys.* **2006**, *124*, No. 204501.
(17) Mathias, G.; Egwolf, B.; Nonella, M.; Tavan, P. *J. Chem. Phys.* **2003**, *118*, 10847.
(18) Mathias, G.; Tavan, P. *J. Chem. Phys.* **2004**, *120*, 4393.
(19) Lorenzen, K.; Schwörer, M.; Tröster, P.; Mates, S.; Tavan, P. *J. Chem. Theory Comput.* **2012**.
(20) Loncharich, R.; Brooks, B. *Proteins: Struct., Funct., Bioinf.* **1989**, *6*, 32−45.
(21) Schreiber, H.; Steinhauser, O. *Biochemistry* **1992**, *31*, 5856−5860.
(22) Schreiber, H.; Steinhauser, O. *Chem. Phys.* **1992**, *168*, 75−89.
(23) Schreiber, H.; Steinhauser, O. *J. Mol. Biol.* **1992**, *228*, 909−923.
(24) Saito, M. *Mol. Simul.* **1992**, *8*, 321−333.
(25) Guenot, J.; Kollman, P. *Journal of computational chemistry* **1993**, *14*, 295−311.
(26) Saito, M. *J. Chem. Phys.* **1994**, *101*, 4055.
(27) Oda, K.; Miyagawa, H.; Kitamura, K. *Mol. Simul.* **1996**, *16*, 167−177.
(28) Norberg, J.; Nilsson, L. *Biophys. J.* **2000**, *79*, 1537−1553.
(29) Patra, M.; Karttunen, M.; Hyvönen, M.; Falck, E.; Lindqvist, P.; Vattulainen, I. *Biophys. J.* **2003**, *84*, 3636−3645.
(30) Beck, D.; Armen, R.; Daggett, V. *Biochemistry* **2005**, *44*, 609−616.
(31) Monticelli, L.; Simões, C.; Belvisi, L.; Colombo, G. *J. Phys.: Condens. Matter* **2006**, *18*, S329.
(32) Reif, M.; Kräutler, V.; Kastenholz, M.; Daura, X.; Hünenberger, P. *J. Phys. Chem. B* **2009**, *113*, 3112−3128.
(33) Ewald, P. *Ann. Phys* **1921**, *64*, 253−287.
(34) Darden, T.; York, D.; Pedersen, L. *J. Chem. Phys.* **1993**, *98*, 10089.
(35) Essmann, U.; Perera, L.; Berkowitz, M.; Darden, T.; Lee, H.; Pedersen, L. *J. Chem. Phys.* **1995**, *103*, 8577−8593.
(36) Frenkel, D.; Smit, B. *Understanding molecular simulation: from algorithms to applications*; Academic Press: San Diego, CA, 2002; Vol. *1*.
(37) Kia, A.; Kim, D.; Darve, E. *J. Comput. Phys.* **2008**, *227*, 8551−8567.
(38) Yokota, R.; Narumi, T.; Barba, L.; Yasuoka, K. *Arxiv preprint* **2011**, No. arXiv:1106.5273.
(39) Andoh, Y.; Okazaki, S. Private communication, 2012.
(40) Barnes, J.; Hut, P. *Nature* **1986**, *324*, 4.
(41) Greengard, L.; Rokhlin, V. *J. Comput. Phys.* **1987**, *73*, 325−348.
(42) Zhou, R.; Berne, B. *J. Chem. Phys.* **1995**, *103*, 9444.
(43) Petersen, H. *J. Chem. Phys.* **1995**, *103*, 3668.
(44) Pollock, E.; Glosli, J. *Comput. Phys. Commun.* **1996**, *95*, 93−110.

(45) Lim, K.; Brunett, S.; Iotov, M.; McClurg, R.; Vaidehi, N.; Dasgupta, S.; Taylor, S.; Goddard, W., III. *J. Comput. Chem.* **1997**, *18*, 501−521.
(46) Figueirido, F.; Levy, R.; Zhou, R.; Berne, B. *J. Chem. Phys.* **1997**, *106*, 9835−9849.
(47) Dimitrov, D.; Raev, N. *J. Electroanal. Chem.* **2000**, *486*, 1−8.
(48) Wang, Z.; Lupo, J.; Patnaik, S.; Pachter, R. *Comput. Theor. Polym. Sci.* **2001**, *11*, 375−387.
(49) Deng, S.; Cai, W. *J. Comput. Phys.* **2007**, *227*, 1246−1266.
(50) Wu, X.; Brooks, B. *J. Chem. Phys.* **2005**, *122*, No. 044107.
(51) Wu, X.; Brooks, B. *J. Chem. Phys.* **2008**, *129*, No. 154115.
(52) Wu, X.; Brooks, B. *J. Chem. Phys.* **2009**, *131*, No. 024107.
(53) Takahashi, K.; Yasuoka, K.; Narumi, T. *J. Chem. Phys.* **2007**, *127*, No. 114511.
(54) Takahashi, K.; Narumi, T.; Yasuoka, K. *J. Chem. Phys.* **2010**, *133*, No. 014109.
(55) Takahashi, K.; Narumi, T.; Yasuoka, K. *Mol. Simul.* **2012**, *38*, 397−403.
(56) Klauda, J.; Wu, X.; Pastor, R.; Brooks, B. *J. Phys. Chem. B* **2007**, *111*, 4393−4400.
(57) Takahashi, K.; Narumi, T.; Yasuoka, K. *J. Chem. Phys.* **2011**, *134*, No. 174112.
(58) Venable, R.; Chen, L.; Pastor, R. *J. Phys. Chem. B* **2009**, *113*, 5855−5862.
(59) Takahashi, K.; Narumi, T.; Yasuoka, K. *J. Chem. Phys.* **2011**, *135*, No. 174108.
(60) Narumi, T.; Ohno, Y.; OkimotoN.Koishi, T.; Suenaga, A.; Futatsugi, N.; Yanai, R.; HimenoR.Fujikawa, S.; Ikei, M.; Taiji, M. *A 55 TFLOPS Simulation of Amyloid forming Peptides from Yeast Prion Sup35 with the Specialpurpose Computer System MDGRAPE-3*, 2006.
(61) Taiji, M. *MDGRAPE-3 Chip: a 165-Gflops Application-Specific LSI for Molecular Dynamics Simulations*, 2004.
(62) Taiji, M.; Narumi, T.; Ohno, Y.; Futatsugi, N.; Suenaga, A.; Takada, N.; Konagaya, A. *A Petaflops Special-Purpose Computer System for Molecular Dynamics Simulations*, 2003.
(63) Berendsen, H.; Grigera, J.; Straatsma, T. *J. Phys. Chem.* **1987**, *91*, 6269−6271.
(64) Swope, W.; Andersen, H.; Berens, P.; Wilson, K. *J. Chem. Phys.* **1982**, *76*, 637.
(65) Andersen, H. *J. Comput. Phys.* **1983**, *52*, 24−34.
(66) Nosé, S. *J. Chem. Phys.* **1984**, *81*, 511.
(67) Hoover, W. *Phys. Rev. A* **1985**, *31*, 1695.